Atlantic hurricane surge response to geoengineering

Moore, John C.; Grinsted, Aslak; Guo, Xiaoran; Yu, Xiaoyong; Jevrejeva, Svetlana; Rinke, Annette; Cui, Xuefeng; Kravitz, Ben; Lenton, Andrew; Watanabe, Shingo; Ji, Duoying

Published in:
Proceedings of the National Academy of Sciences of the United States of America

DOI:
10.1073/pnas.1510530112

Published: 10.11.2015

Document Version
Publisher's PDF, also known as Version of record

Citation for pulished version (APA):
Moore, J. C., Grinsted, A., Guo, X., Yu, X., Jevrejeva, S., Rinke, A., Cui, X., Kravitz, B., Lenton, A., Watanabe, S., & Ji, D. (2015). Atlantic hurricane surge response to geoengineering. *Proceedings of the National Academy of Sciences of the United States of America*, *112*(45), 13794-13799. https://doi.org/10.1073/pnas.1510530112

Atlantic hurricane surge response to geoengineering

John C. Moore[a,b,1], Aslak Grinsted[a,c], Xiaoran Guo[a], Xiaoyong Yu[a], Svetlana Jevrejeva[a,d], Annette Rinke[a,e], Xuefeng Cui[a], Ben Kravitz[f], Andrew Lenton[g], Shingo Watanabe[h], and Duoying Ji[a,1]

[a]Joint Center for Global Change Studies, College of Global Change and Earth System Science, Beijing Normal University, Beijing 100875, China; [b]Arctic Centre, University of Lapland, Rovaniemi 96101, Finland; [c]Centre for Ice and Climate, Niels Bohr Institute, University of Copenhagen, 2100 Copenhagen Ø, Denmark; [d]National Oceanography Centre, Liverpool L3 5DA, United Kingdom; [e]Alfred Wegener Institute, Helmholtz Centre for Polar and Marine Research, Potsdam 14473, Germany; [f]Atmospheric Sciences and Global Change Division, Pacific Northwest National Laboratory, Richland, WA 99352; [g]Commonwealth Scientific and Industrial Research Organisation, Oceans and Atmosphere Flagship, Hobart, Tasmania, TAS 7004, Australia; and [h]Japan Agency for Marine-Earth Science and Technology, Yokohama 237-0061, Japan

Edited by Kerry A. Emanuel, Massachusetts Institute of Technology, Cambridge, MA, and approved September 29, 2015 (received for review June 12, 2015)

Devastating floods due to Atlantic hurricanes are relatively rare events. However, the frequency of the most intense storms is likely to increase with rises in sea surface temperatures. Geoengineering by stratospheric sulfate aerosol injection cools the tropics relative to the polar regions, including the hurricane Main Development Region in the Atlantic, suggesting that geoengineering may mitigate hurricanes. We examine this hypothesis using eight earth system model simulations of climate under the Geoengineering Model Intercomparison Project (GeoMIP) *G3* and *G4* schemes that use stratospheric aerosols to reduce the radiative forcing under the Representative Concentration Pathway (RCP) 4.5 scenario. Global mean temperature increases are greatly ameliorated by geoengineering, and tropical temperature increases are at most half of those temperature increases in the RCP4.5. However, sulfate injection would have to double (to nearly 10 teragrams of SO_2 per year) between 2020 and 2070 to balance the RCP4.5, approximately the equivalent of a 1991 Pinatubo eruption every 2 y, with consequent implications for stratospheric ozone. We project changes in storm frequencies using a temperature-dependent generalized extreme value statistical model calibrated by historical storm surges and observed temperatures since 1923. The number of storm surge events as big as the one caused by the 2005 Katrina hurricane are reduced by about 50% compared with no geoengineering, but this reduction is only marginally statistically significant. Nevertheless, when sea level rise differences in 2070 between the RCP4.5 and geoengineering are factored into coastal flood risk, we find that expected flood levels are reduced by about 40 cm for 5-y events and about halved for 50-y surges.

extremes | flooding | climate engineering

Changes in the frequency and intensity of extreme events, such as droughts, storms, floods, volcanic eruptions, and earthquakes, are generally likely to have more of an impact on the environment, human activities, and economies than changes in mean climate. The most intense floods are associated with tropical events, such as typhoons or hurricanes, because the strong winds and intense low pressure associated with tropical cyclones generate storm surges (1–3). Damage to coastal cities is the greatest cost from increased sea level rise and flooding risk (2, 4). Several of the largest cities in the United States are vulnerable to the Atlantic surge threat, such as those surges caused by Hurricane Katrina (2005) or Superstorm Sandy (2012).

Atlantic hurricanes are not simply stochastic events, but are statistically related to large-scale climate phenomena, such as the state of El Niño Southern Oscillation (ENSO) (5), North African dust (6), and, most clearly, global and tropical Atlantic temperatures (7). Geoengineering is a method of offsetting the global temperature rise from greenhouse gases, although inevitably also altering other important climate parameters, such as precipitation and teleconnection patterns (8, 9). We may thus ask the question: How successful would geoengineering be at reducing the frequency and intensity of hurricane storm surges from Atlantic hurricanes? To date, analyzing extremes under geoengineering scenarios has been limited (10) due to the relatively short (typically 50 y) duration of simulations and, in the case of intense storms or hurricanes, by the relatively low resolution of climate models.

The influence of climate change on Atlantic hurricanes has been difficult to establish: Visual observations of storms were spatially confined to near coastal areas until the satellite era, climate models have generally been of too coarse a resolution to resolve hurricanes adequately, and no ab initio model of hurricane formation exists as of yet. A relatively new and unbiased observational index of storm surges recorded in six high-frequency tide-gauge records extending back to 1923 from the southeastern United States (3) (*Methods*) shows that the frequency and magnitude of storm surges varied with temperature. Warmer sea surface temperatures raise the ocean-atmospheric thermodynamic state, increasing the maximum potential tropical cyclone frequency and intensity. However, warming may also dry the middle troposphere and increase vertical wind shear, reducing cyclone numbers (11), although some studies find this latter effect to be minor (12). Genesis potential indices (12, 13) empirically combine these factors to relate tropical cyclone cyclogenesis to environmental forcing factors. Genesis potential dependence on sea surface temperature changes appears similar whether caused by either increased atmospheric CO_2 concentrations or changes in insolation at the 1–2 °C range discussed here (13), but aerosol effects that may be relevant to geoengineering were not simulated. Geoengineering by injection of sulfate aerosols into the lower stratosphere would result in increased absorption of solar radiation and localized heating. Increasing concentrations of greenhouse gases, to the contrary, leads to cooling of the tropical tropopause and lower stratosphere. This region of the atmosphere controls the outflow temperature of tropical cyclones, with warmer outflow temperatures associated with a decrease in tropical cyclone intensity (14). Despite these complicating factors, Grinsted et al. (7)

Significance

We estimate that stratospheric sulfate aerosol geoengineering may somewhat ameliorate Atlantic hurricane intensity and frequency, but there will be more "Katrina"-level events than during the past 30 y. Geoengineering would likely be reasonably effective at controlling coastal flood risk relative to the coastal flood risk expected under the Representative Concentration Pathway (RCP) 4.5 greenhouse gas warming, in part, due to its impact on global sea level rise, although flood risk would still be significantly larger than at present.

Author contributions: J.C.M. designed research; J.C.M., A.G., B.K., A.L., S.W., and D.J. performed research; A.G. contributed new reagents/analytic tools; A.G., X.G., X.Y., and D.J. analyzed data; and J.C.M., S.J., A.R., X.C., and B.K. wrote the paper.

The authors declare no conflict of interest.

This article is a PNAS Direct Submission.

[1]To whom correspondence may be addressed. Email: duoyingji@bnu.edu.cn or john.moore.bnu@gmail.com.

This article contains supporting information online at www.pnas.org/lookup/suppl/doi:10.1073/pnas.1510530112/-/DCSupplemental.

showed that globally gridded surface temperatures, temperatures in the tropical Atlantic Main Development Region (MDR; 85°W–20°W and 10°N–20°N), and simple global mean surface temperature all explain Atlantic hurricane observations better than various predictors previously suggested, such as the North Atlantic Oscillation, Southern Oscillation, radiative forcing, and MDR temperature anomaly relative to tropical ocean temperatures. Results from downscaling global climate model output to generate hurricane statistics under changing climate have been published (ref. 15 and references therein); only one method (15) finds increases in North Atlantic tropical cyclone numbers through the 21st century, whereas other approaches predict decreases. Robust temperature differences between geoengineered and greenhouse climates (9) (*Results*) motivate us to use a temperature-dependent generalized extreme value (GEV) model of cyclone probability density function (7) rather than counts of poorly resolved cyclones or changes in vertical wind shear. This model also allows both the cyclone intensity and its frequency to be related to regional or global temperatures.

Results

We use the homogeneous surge index (3) and the nonstationary GEV model (7), with shape (k), scale (σ), and location (μ) parameters dependent on temperature (T). The location and scale parameters are primarily related to the size and frequency of surges occupying the central part of the storm surge probability distribution, and so describe medium-sized storms, whereas the shape parameter determines the "fat-tail" of the distribution, and so controls the frequency of the most extreme storms. Choice of T is quite flexible; here, we use mean global (or MDR) surface temperatures or the full set of gridded surface temperatures from the different climate ensembles. In the case of the gridded temperature field, each spatial grid cell contributes its own GEV model, which is weighted by its area and Bayesian likelihood relative to the GEV model using global mean temperature. Each of the GEV parameters is related to T as follows:

$$\begin{aligned} k &= k_0(1+a_k T) \\ \sigma &= e^{s_0(1+a_s T)} \\ \mu &= \mu_0(1+a_\mu T). \end{aligned} \qquad [1]$$

In Eq. **1**, k_0, s_0, and μ_0 are values of the GEV parameters for an arbitrary baseline climate where $T = 0$, whereas the coefficients of T (a_k, a_s, and a_μ) describe how sensitive the distribution is to changes in T. The analytical form for the nonstationary parameters is chosen for convenience, with positive values associated with (*i*) more frequent extreme surges expressed by k, (*ii*) a broader distribution reflected by σ, and (*iii*) an increase in the size of peak storm surge indicated by μ. We estimate the six parameters (*Methods*) and map the temperature-dependent coefficients in Fig. 1.

With the parameter values found for the GEV over the surge index record, which starts in 1923, we can then estimate the GEV distribution, given values of T in Eq. **1**, and thereby reconstruct and project the storm surge probability distribution over time. The surge index is normalized using the highest surge recorded during Hurricane Katrina in 2005 as a benchmark for extremes. Extreme events crossing this threshold are labeled as "Katrinas" (*Methods*). The GEV model used is based on historical observations and patterns between temperatures, surge frequency, and severity. However, observed teleconnections are consistent with the patterns seen in Fig. 1 (7). In a geoengineered world, both greenhouse gases and stratospheric aerosol forcing occur simultaneously, whereas, this pairing only occurs during transient volcanic eruptions in the historical record.

Both of the Geoengineering Model Intercomparison Project (GeoMIP) scenarios we use here, *G3* and *G4* (*Methods*), lead to

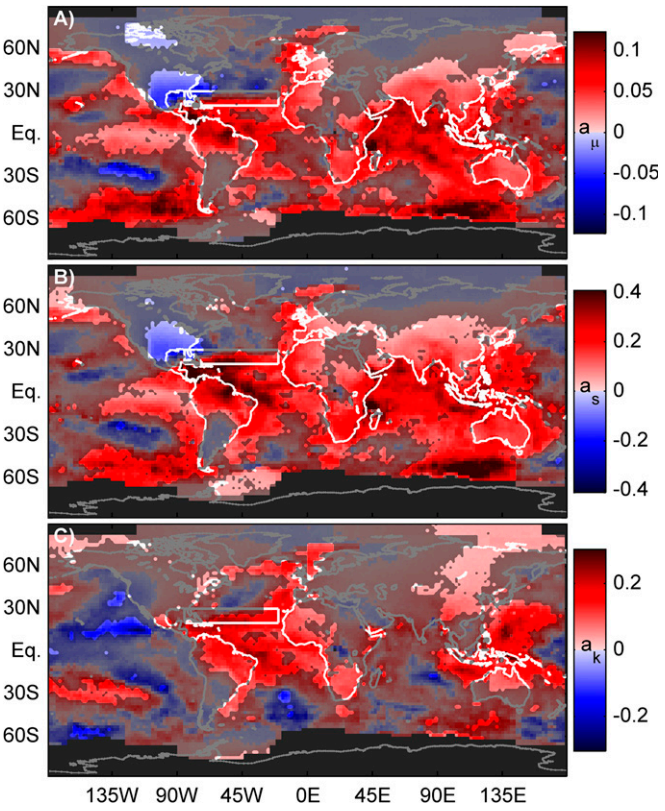

Fig. 1. GEV teleconnection patterns between gridded surface temperatures and surge index. The MDR is marked by a rectangle. Coefficients describe modal sensitivity (a_μ) (*A*), spread (a_s) (*B*), and the high-impact tail (a_k) (*C*) of the GEV distribution as a function of local temperature (T) in Eq. **1**. Black indicates insufficient data, and gray indicates regions where the 5–95% confidence interval spans zero (where the coefficient is not significant). Red values indicate regions where locally increased T means greater Atlantic storm surge magnitude or variance. Blue implies the opposite relations. Red values over the MDR suggest rising MDR temperature drives increased numbers of more intense storms, whereas blue values over the southeastern United States suggest cooling by those storms as they make landfall.

modest warming almost everywhere relative to temperatures in the baseline climate, which we take as the *rcp45* temperatures [i.e., model-simulated temperatures when forced by the Representative Concentration Pathway (RCP) 4.5 scenario] over the 2010–2029 interval (Fig. 2). Between 2050 and 2069, global surface air temperatures warm by 1.3 °C in *rcp45*, by 0.48 °C with *G3*, and by 0.79 °C with *G4* relative to 2010–2029. Over the same interval, MDR temperatures warm by 0.8 °C, 0.2 °C, and 0.4 °C with *rcp45*, *G3*, and *G4*, respectively. *G3* in the HadGEM2-ES and BNU-ESM models succeeds in stabilizing both MDR and global temperatures from 2020 to 2070. The general pattern of temperature change under all three scenarios includes accentuated Arctic warming, less warming over the oceans than on land outside the Arctic, and the least warming in the tropics. The main effect of geoengineering seems to be in reducing land temperature rises relative to *rcp45*, and hence in reducing the difference in warming between land and oceans expected under *rcp45* by ∼1 °C.

Most models agree on warming under both *G3* and *G4* in the regions of the North Atlantic Drift and subtropical South America. Fig. 1 shows how the temperatures in these two regions are statistically useful predictors of the GEV shape parameter, a_k, which is related to the high-intensity (hurricane) end of the storm surge distribution. Subtropical South America has a positive association with a_k, and the North Atlantic Drift has a negative association (although this latter feature is not statistically significant at the 95%

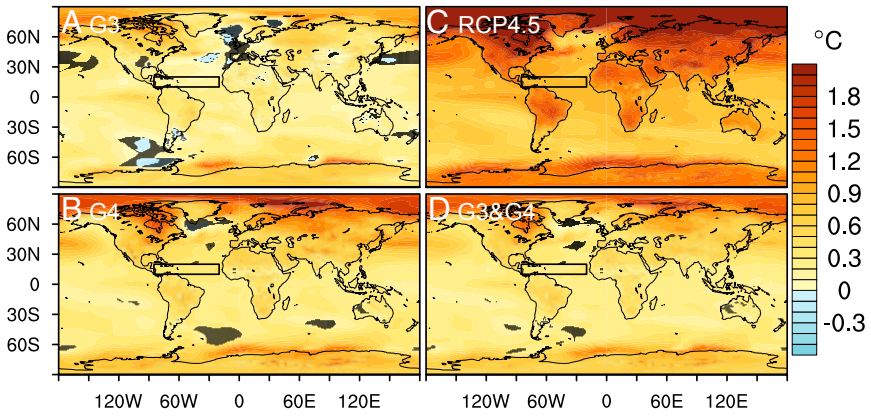

Fig. 2. Mean surface air temperature anomalies during 2050–2069 simulated under *G3*: an ensemble consisting of BNU-ESM (42), HadGEM2-ES (43), and IPSL-CM5A-LR (44) models (*Methods*) (*A*); *G4*: an ensemble consisting of BNU-ESM, CanESM2 (45), CISRO-Mk3L (46), GISS-E2-R (47), HadGEM2-ES, MIROC-ESM (48), and MIROC-ESM-CHEM (48) models (*B*); *rcp45*: an ensemble consisting of the eight different models that ran *G3* or *G4* (*C*); and the combined *G3&G4* ensemble of the 10 model simulations of *G3* and *G4* (*D*). Anomalies are relative to the baseline *rcp45* climate state between 2010 and 2029. The MDR is marked by a black rectangle. Stippling indicates where fewer than six of eight *rcp45*, two of three *G3*, five of seven *G4*, or seven of 10 combined *G3&G4* climate simulations agree on the sign of the change. Figs. S1 and S2 show each model's anomalies.

level). Thus, a rise in temperature in subtropical South America would statistically suggest more intense hurricanes, but would tend to be counteracted by rising temperatures in the mid-North Atlantic. Arid regions (Australia, North Africa, and Northwest China) all warm in both *rcp45* and geoengineering ensembles, but by much less with geoengineering than without, and all are associated with increased hurricane extremes (Fig. 1). The other regions where significant teleconnections were found, such as the tropical Atlantic and western Pacific (Fig. 1), also show similar patterns of warming, although magnitudes are reduced with geoengineering compared with the *rcp45* ensemble (Fig. 2). The teleconnection pattern for other two GEV distribution terms (Fig. 1) has positive factors over more of the tropical oceans than does a_k. This association suggests that the total numbers of Atlantic cyclones and the spread of their sizes would rise as tropical oceans warmed, even if their extremes behave more complexly.

Applying the hurricane GEV model to *G3* and *G4* scenarios produces similar results for the extreme event tail (Fig. 3), although it is clearly seen that *G3* is more successful at maintaining temperatures and Katrinas at levels similar to levels in 2010. There is also a more obvious termination shock under *G3* than *G4* due to a larger geoengineering forcing in *G3* than in *G4*. The *G4* ensemble-gridded model exhibits a pronounced peak around 2010–2020, which is much less noticeable in the global and MDR models. This feature is not due to any one model in particular (Fig. S4), however, and the linear trend from 2000 to 2070 would pass through the 16–84% confidence interval, so this feature is not statistically significant. The *G3* results fall comfortably within the confidence interval of *G4*, suggesting that we may usefully group *G3* and *G4*, gaining some statistical confidence in the increased size of the ensemble. The similarity of the *G3* and *G4* regional patterns of climate response of various regional climate indices has been noted previously (16).

Risk analysis and coastal defense planning must combine surge levels with expected rises in mean sea level (2, 17). In Fig. 4, we illustrate how this combination may have an impact on two locations (Atlantic City and Pensacola) using historical storm surges and temperatures. Separating the tide gauge data into globally cold and warm years reveals that warm years have been associated with a dramatic increase in the frequency of extreme storm surges (Fig. 4). Global temperature differences between the warm and cold years in the historical record are rather similar to average differences projected between *rcp45* and *G4*. The spatial variability of future warming will be different from the past (Fig. 2), but for a first approximation, we may assume a similar storm sensitivity; that is, the spatial GEV coefficients (Fig. 1) will remain stationary. In other words, we could conservatively accept the null hypothesis that there is no difference between extremes under geoengineering or greenhouse gas forcing (compare Fig. 3). Then, surge levels at 2070 are found by adding the sea level rise expected under the RCP4.5 (17), or under *G4*, which is about 50% lower than RCP4.5 levels (4). The difference in surge threat between the RCP4.5 and *G4* varies considerably between Atlantic City and Pensacola, especially at the more uncertain high-flood-risk tail of the distribution. At both locations, 5-y events are associated with ~40-cm higher surges under the RCP4.5 than with *G4*. A 50-y flood in Atlantic City is almost halved in magnitude by geoengineering, whereas the difference is very uncertain and not significant in Pensacola. Analysis of eight other long-term tide-gauge records (Fig. S5) shows that the surge distributions are usually well separated, as for Atlantic City, with overlapping confidence intervals only for rare events at a few locations.

Discussion

Because hurricane numbers depend strongly on warming temperatures, especially in tropical regions, we may expect that *G3* and *G4* will lead to somewhat reduced hurricane numbers relative to *rcp45*. The *rcp45* ensemble does indeed lead to higher numbers of Katrinas with the GEV model than do *G3* and *G4* (Fig. 3) between 2020 and 2070, because both MDR and global temperatures are warmer than under *G3* and *G4*. However, the difference is rather small and not outside the confidence interval, except for the combined *G3 & G4* ensemble. Larger numbers of Katrinas are present throughout the 2020–2070 geoengineering interval compared with the present day, except for the *G3* scenario driven by MDR temperatures. The difference in numbers of Katrinas according to the combined ensemble under geoengineering compared with the RCP4.5 is about a factor of 2, is similar for all three temperature metrics modeled, and may be said to be marginally significant (around $P = 0.1$).

In a geoengineered climate, the teleconnection patterns that are useful statistical indicators of hurricanes (e.g., 5, 6, 18) are likely to be altered as the long-wave greenhouse gas and short-wave aerosol radiative forcing patterns produce changes in latitudinal, seasonal, diurnal, terrestrial, and oceanic heating patterns (19). These teleconnections are implicit in the GEV model relationships

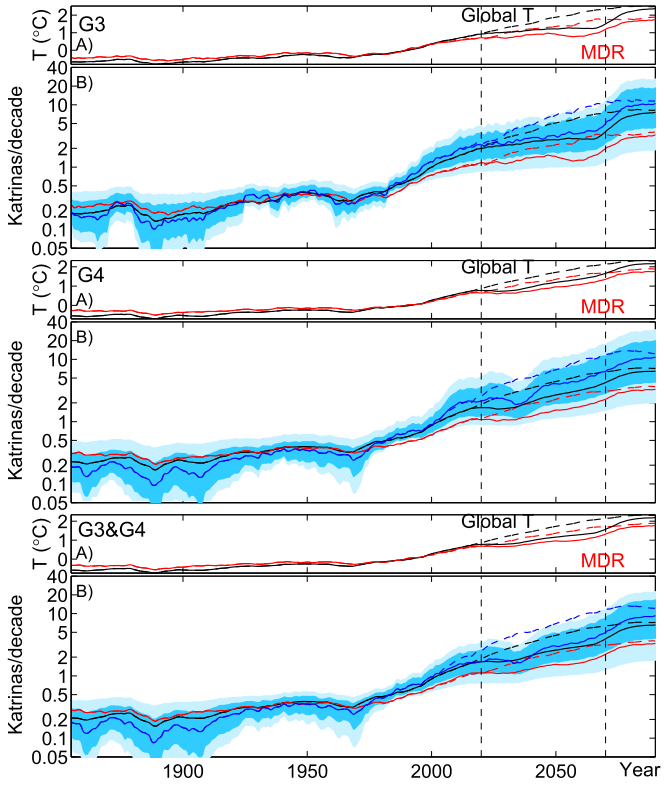

Fig. 3. Number of Katrina-magnitude surge events per decade (*B*) under the projected changes in temperatures under the *G3* (*Top*), *G4* (*Middle*), and combined *G3&G4* (*Bottom*) geoengineering ensembles and with the same models running the RCP4.5 forcing scenarios shown by the temperatures in *A*. The vertical dashed lines indicate the period 2020–2070 during which the geoengineering is applied. Solid lines indicate results under geoengineering, and dashed lines indicate results under RCP4.5; blue lines show the projection using the full spatial-gridded temperatures and confidence interval (5–16–84–95%); and red and black lines show the projections using only MDR and global average surface temperature, respectively. Figs. S3 and S4 show individual model simulations.

for globally gridded observations of past temperature (Fig. 1) that Grinsted et al. (7) found to be the best predictor of hurricanes. Recent work (14) suggests that other factors, such as stratospheric ozone depletion due to the presence of substantial stratospheric chlorofluorocarbons (CFCs), may already be playing a role in hurricane formation. Although CFC concentrations are decreasing, they will remain significant until about 2060, and stratospheric sulfate injections, while they are present, would exacerbate ozone depletion (20). Hence, some doubt must be attached to the gridded temperature predictor model.

One clear teleconnection pattern for a_k is with Amazonian temperatures (Fig. 1). The outflow of the Amazon and Orinoco Rivers mixes with surface waters of the tropical Atlantic, such that 68% of the largest category hurricanes pass over the plume (21). This freshwater plume inhibits the mixing of colder water beneath the surface and raises surface ocean temperatures, thus generally increasing hurricane intensity and likelihood. Precipitation in *rcp45*, *G3*, and *G4* is slightly reduced by about 2% over the Amazon in the GeoMIP model simulations, which is not significant, so the freshwater plume is unlikely to be substantially different in the future scenarios studied here. A second clear pattern associated with the extreme event end of the hurricane distribution is the negative correlation with western Pacific temperatures associated with the ENSO hurricane pattern (5) governed by Rossby waves generated over the Pacific. There is, however, a general positive correlation between warming tropics and numbers of smaller storm surges, as indicated by the maps for a_s and a_μ (Fig. 1). The ability of climate models to simulate ENSO variability is improving, but predicting its response to warming still remains relatively uncertain (22). The linkage with arid region conditions has been noted for the African Sahel, likely through dust affecting Atlantic surface isolation by both direct aerosol effect and indirect aerosol effects changing cloud cover (23, 24). The other arid regions may be simply covarying with North African conditions or indicating the widespread importance of dust effects on climate. If the tropical Atlantic MDR could be preferentially cooled, damage from hurricanes may well be reduced.

The explosive volcanic eruptions of Katmai (Alaska, June 1912) and El Chichon (Mexico, April 1982) preferentially loaded the Northern Hemisphere with aerosol, and they were followed by the least active hurricane season on record in 1914 and the least active hurricane season in the satellite observation period in 1983 [HURDAT2 (25)]. These observations suggest that injecting stratospheric aerosols into the Northern Hemisphere may mitigate Atlantic hurricanes. Haywood et al. (26) used the HadGEM2-ES model to simulate injection of 5 teragrams (Tg) of SO_2 per year (as for *G4*) into only the Northern Hemisphere stratosphere. Previous modeling on the impacts of volcanic eruptions suggests that the Intertropical Convergence Zone (ITZC) moves away from the cooler hemisphere (24), shifting the African monsoon circulation and, crucially in the HadGEM2-ES Northern Hemisphere geoengineering simulation, the precipitation of the water-stressed Sahel region. The southward shift of the ITCZ would likely also affect runoff in Amazonia, altering ocean mixing of cold water to the surface in the tropical Atlantic, as described previously. Stratospheric aerosol geoengineering results in a longer westerly phase of the Quasi-Biennial Oscillation (QBO) (27), and with

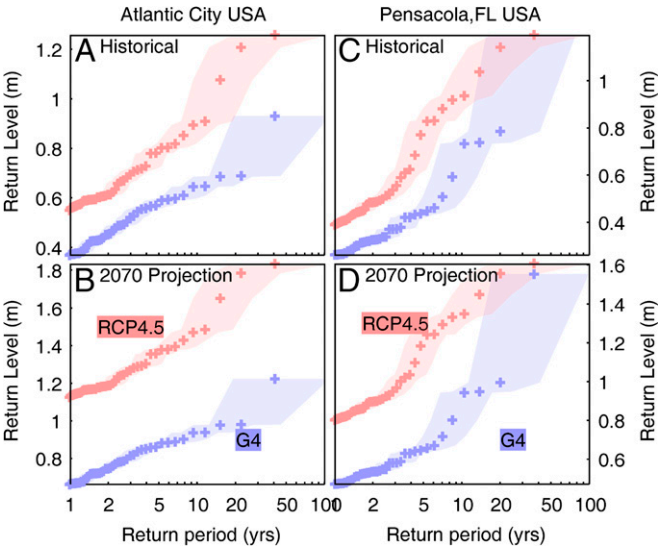

Fig. 4. (*Top*) Storm surge return periods from daily tide gauge data at Atlantic City (*A*) and Pensacola (*C*) since 1911 and 1923 divided into globally relatively warm (red) and cool (blue) years, along with their 16–84% confidence ranges [shaded bands based on the Jeffreys interval estimator (49)]. (*Bottom*) Return period ranges at 2070 under RCP4.5 (red) and *G4* (blue) for Atlantic City (*B*) and Pensacola (*D*) relative to mean sea level over 1990–2010. Return levels at 2070 were estimated taking into account local land subsidence, plus the 50th percentile rises forecast at the tide gauge sites for 2070 estimated under RCP4.5 (18) or *G4* (4). The differences between global (MDR) warm and cold year mean temperatures over the historical period are 0.42 °C (0.37 °C) from observations (38) and 0.37 °C (0.31 °C) from the models used here (legend for Fig. 2). This difference compares with simulations of the global (MDR) temperature differences in the years 2020–2070 between *rcp45* and the *G4* ensembles of 0.56 °C (0.37 °C).

sufficient injection magnitude, a locking of the QBO in its westerly phase, which are effects not included in the hemispheric geoengineering simulation (26). The westerly phase is characterized by stronger poleward aerosol transport (28, 29). Moreover, local heating of aerosols enhances cross-hemispheric aerosol transport (30); aerosols from the 1982 El Chichon eruption were observed in Antarctica (31). Hence, whether stratospheric sulfate aerosol geoengineering can be isolated to a single hemisphere is, at present, inconclusive.

The GEV relations found for the global mean and the MDR temperature are almost as good predictors as the gridded temperatures (7). Formation of hurricanes is complex (1, 11–15), but because they form in the tropical Atlantic, conditions there (especially sea surface temperatures) are the most proximate factor in hurricane variability. Hence, the MDR temperature is perhaps the most robust indicator of the hurricane probability distribution in a geoengineered world. Fig. 3 shows that the MDR temperature signal changes less than global temperatures in both *rcp45* and the geoengineering ensemble, but this lack of sensitivity also means that the tropical Atlantic is one of the regions least affected by global stratospheric aerosol geoengineering. Nevertheless, a rise in Katrina event likelihood is predicted under both the RCP4.5 and geoengineering scenarios compared with the present.

Conclusions

An arguably realistic formulation of geoengineering by sulfate aerosol injection does cause tropical Atlantic temperatures to rise more slowly than without geoengineering. For hurricanes, this relative cooling is a key determining factor for both frequency and intensity because, according to the GEV model (7), both rise very quickly with warming temperatures. Alternative estimates of tropical storm intensity, such as genesis potential, tend to show much smaller trends with temperature (15). Earth system model results based on these measures depend on model convection scheme parameterizations and appropriate selections of representative levels in both atmosphere and ocean (15). Additionally, across-model scatter for stratospheric aerosol simulations is increased because of the different ways in which models handle atmospheric chemistry and how that interacts with their physical convection schemes. Preliminary investigation of potential intensity and genesis potential under the GeoMIP scenarios indicates considerable across-model differences and large temporal variability with, as yet, no consistent pattern emerging of the geoengineering response.

GEV model simulations using temperatures from three earth system models of aerosol injection under *G3* show that Katrina-level storms may be kept at frequencies similar to the present by geoengineering, although confidence intervals overlap with results from *rcp45*. *G4*-simulated temperatures lead to relatively small (50%) and marginally significant changes in Katrina-level events relative to the situation without geoengineering. Damage to coastal infrastructure, however, will likely be dramatically reduced (by halving flood levels) under a *G4* scenario rather than simply following RCP4.5. The 5 Tg of SO_2 per year specified in *G4* approximates to the equivalent of a 1991 Mount Pinatubo volcanic eruption every 4 y (32). *G3* ramps up the sulfate injection, so by 2069, about twice this amount needs to be put into the stratosphere (e.g., 9.8 Tg for the BNU-ESM), depending on the sensitivity of the particular model to stratospheric sulfate aerosols. As levels of SO_2 injections increase, particles coagulate more and fall out of the stratosphere more quickly (33), suggesting sublinear effectiveness of aerosol loading. It is doubtful whether aerosol injection can be done in sufficient quantities to balance radiative forcing from, for example, the RCP8.5 greenhouse gas emission scenario (34). Furthermore, sulfate aerosol geoengineering would affect stratospheric chemistry (20), potentially complicating the simple temperature dependencies modeled here (14). In considering a geoengineered world, it is also important to remember that the alternative is likely to be one with high CO_2 concentrations rather than a preindustrial climate. In both high-CO_2 and geoengineered worlds, regional differences in climate would likely be larger than today (9, 16, 35), but the extent of regional differences exacerbated by greenhouse gas forcing could potentially be moderated with geoengineering. Targeting the northern tropical stratosphere, while preferentially cooling the tropical Atlantic and lowering hurricane risk, would, however, also likely cause shifts in the ITCZ, exacerbating drought conditions in the Sahel (26).

Geoengineering by global stratospheric sulfate injection appears to ameliorate Atlantic hurricanes, and additionally mitigates coastal flooding via reduced rates of sea level rise. However, model results suggest this reduced flood risk could require rather large sulfate injections (*G3* simulations suggest the equivalent of a Pinatubo eruption every 2 y) by 2070 even under the modest RCP4.5 scenario. Even this extreme level of aerosol injection will not return the world to 20th century levels of hurricane risk. Hence, we conclude from our results that unless better storm surge protection measures are made, there will be considerable increases in damage to the coastal infrastructure through the 21st century.

Methods

The storm surge index is defined as the multiple tide gauge station daily maximum of deseasonalized squared day-to-day differences in sea level (3). This index is designed to be sensitive to (*i*) large-scale sea level disturbances rather than local flood levels, which depend strongly on coastal geometry, and (*ii*) the slower large-scale ocean swells associated with the hurricane surge. Normalization by Hurricane Katrina was criticized (36) because tide gauges may be located far away from landfall locations, but the surge index does primarily respond to intense land-falling cyclones (3, 37). We emphasize that a storm surge of this magnitude will have very variable impacts depending on where it makes landfall and what levels of flood protection are in place, and that the storm surge index is not a proxy for wind speed but for the coastal surge threat.

GEV Parameter Estimation. Grinsted et al. (7) estimated the six unknown parameters in Eq. **1** and their confidence intervals using Markov chain Monte Carlo methods to examine the likelihood density of the parameter space. We use the historical record of storm surges (3), with the observed surface temperatures (38) as the predictor, *T*, in Eq. **1** to produce the map of GEV temperature coefficients (Fig. 1). For global and MDR temperatures, the estimated parameters are all significantly different from zero, but when using gridded temperatures, only relatively small regions have a clearly defined impact on Atlantic surge index (Fig. 1); that is, most regional temperatures are much worse predictors of hurricanes than global mean temperatures. This behavior is consistent with several known teleconnection patterns (5, 6, 18) related to Atlantic hurricanes.

Climate Model Forcing Setup. We make use of the *G3* and *G4* GeoMIP solar radiation management scenarios (39). *G3* and *G4* specify an injection of sulfate aerosol into the tropical lower stratosphere (altitude of 16–25 km) that either balances increases in greenhouse gas-induced radiative forcing specified by the RCP4.5 scenario (*G3*) or envisages a constant injection rate of 5 Tg of SO_2 per year (*G4*). Both experiments run geoengineering for 50 y starting in 2020. Following cessation of geoengineering in 2069, the scenarios run for a further 20 y to provide information on the so-called "termination effect" (40). We analyzed three models that have completed the *G3* experiment and seven models simulating *G4*; eight models have run at least one of them, and 10 simulations were done in total. The Coupled Model Intercomparison Project Phase 5 (CMIP5) experiment *rcp45*, which is the future climate state forced by the RCP4.5 (41), is the reference climate we use for comparison. The *G3* and *G4* scenarios begin in 2020, and so we use the CMIP5 *historical* and *rcp45* model runs to produce continuous time series of climate change from 1850 to 2090. For each of the three model ensembles (i.e., *G3*, *G4*, *G3&G4*; as listed in the legend for Fig. 2), we also create corresponding ensembles containing the same model simulations of *historical* and *rcp45*. Because climate has not been, and will not be, stationary, we need to select a reference period that is long enough for reliable climatology but still

leaves significant climate change under the RCP4.5 by 2070; hence, we use the 2010–2029 interval as our reference climate.

Other model fields, such as precipitation under *G3* and *G4*, show much less significant regional differences than do temperature anomalies (16, 35). Furthermore, under geoengineering, there are smaller changes in precipitation compared with preindustrial precipitation than under purely greenhouse gas forcing (8, 16); this effect is related to much smaller temperature-driven feedbacks in the climate system under geoengineering than under pure greenhouse gas forcing (19). These smaller feedbacks would imply that a geoengineered high-CO_2 world may be closer to our present climate than a purely greenhouse gas-forced world in terms of hurricane frequency, which is, of course, one potential objective of geoengineering; hence, the GEV model parameters or the surge threat found from the historical period are as plausible in *G3* and *G4* as they are under the RCP4.5.

We also examined daily two- to six-bandpass filtered sea level pressure variability, wind shear, thermodynamic potential intensity, and genesis potential (14, 15) over the MDR region in earth system model output for changes that could characterize changes in cyclone activity. We found no significant differences, which may perhaps be expected, given the relatively low resolution (≈200 km) of the models compared with tropical cyclones.

ACKNOWLEDGMENTS. We thank J. Haywood and A. Jones, the editor, and two anonymous referees for suggesting improvements to the manuscript; all participants of the GeoMIP and their model development teams; the CLIVAR/WCRP Working Group on Coupled Modeling for endorsing the GeoMIP; and the scientists managing the earth system grid data nodes who have assisted with making GeoMIP output available. This research was funded by the National Basic Research Program of China (Grant 2015CB953600). The Pacific Northwest National Laboratory is operated for the US Department of Energy by Battelle Memorial Institute under Contract DE-AC05-76RL01830. GISS ModelE2 simulations were supported by the National Aeronautics and Space Administration (NASA) High-End Computing Program through the NASA Center for Climate Simulation at the Goddard Space Flight Center. S.J. was funded by the European Union's Seventh Programme for Research, Technological Development and Demonstration under Grant FP7-ENV-2013-Two-Stage-603396- RISES-AM. A.L. was supported by the Commonwealth Scientific and Industrial Research Organisation Oceans, Atmosphere Flagship, and S.W. was supported by the SOUSEI Program, Ministry of Education, Culture, Sports, Science and Technology, Japan.

1. Knutson TR, et al. (2010) Tropical cyclones and climate change. *Nat Geosci* 3:157–163.
2. Lin N, Emanuel K, Oppenheimer M, Vanmarcke E (2012) Physically based assessment of hurricane surge threat under climate change. *Nat Clim Change* 2:462–467.
3. Grinsted A, Moore JC, Jevrejeva S (2012) Homogeneous record of Atlantic hurricane surge threat since 1923. *Proc Natl Acad Sci USA* 109(48):19601–19605.
4. Moore JC, Jevrejeva S, Grinsted A (2010) Efficacy of geoengineering to limit 21st century sea-level rise. *Proc Natl Acad Sci USA* 107(36):15699–15703.
5. Gray WM (1984) Atlantic seasonal hurricane frequency. Part I: El Niño and 30 mb quasi-biennial oscillation influences. *Monthly Weather Review* 112(9):1649–1668.
6. Gray WM (1990) Strong association between west african rainfall and u.s. Landfall of intense hurricanes. *Science* 249(4974):1251–1256.
7. Grinsted A, Moore JC, Jevrejeva S (2013) Projected Atlantic tropical cyclone threat from rising temperatures. *Proc Natl Acad Sci USA* 110(14):5369–5373.
8. Tilmes S, et al. (2013) The hydrological impact of geo-engineering in the Geoengineering Model Intercomparison Project (GeoMIP). *J Geophys Res* 118(19): 11036–11058.
9. Ricke KL, Morgan MG, Allen MR (2010) Regional climate response to solar-radiation management. *Nat Geosci* 3:537–541.
10. Curry CL, et al. (2014) A multi-model examination of climate extremes in an idealized geoengineering experiment. *J Geophys Res* 119(7):3900–3923.
11. Vecchi GA, Soden BJ (2007) Increased tropical Atlantic wind shear in model projections of global warming. *Geophys Res Lett* 34:L08702.
12. Bruyère C, Holland G, Towler E (2012) Investigating the use of a Genesis Potential Index for tropical cyclones in the North Atlantic Basin. *J Clim* 25(24):8611–8626.
13. Emanuel K, Sobel A (2013) Response of tropical sea surface temperature, precipitation, and tropical cyclone-related variables to changes in global and local forcing. *Journal of Advances in Modeling Earth Systems* 5(2):447–458.
14. Emanuel K, Solomon S, Folini D, Davis S, Cagnazzo C (2013) Influence of tropical tropopause layer cooling on Atlantic hurricane activity. *J Clim* 26:2288–2301.
15. Emanuel KA (2013) Downscaling CMIP5 climate models shows increased tropical cyclone activity over the 21st century. *Proc Natl Acad Sci USA* 110(30):12219–12224.
16. Yu X, et al. (2015) Impacts, effectiveness and regional inequalities of the GeoMIP G1 to G4 solar radiation management scenarios. *Global Planet Change* 129:10–22.
17. Kopp RW, et al. (2014) Probabilistic 21st and 22nd century sea-level projections at a global network of tide gauge sites. *Earth's Future* 2:383–406.
18. Moore JC, Grinsted A, Jevrejeva S (2008) Gulf stream and ENSO increase the temperature sensitivity of Atlantic tropical cyclones. *J Clim* 21(7):1523–1531.
19. Kravitz B, et al. (2013) An energetic perspective on hydrologic cycle changes in the Geoengineering Model Intercomparison Project (GeoMIP). *J Geophys Res* 118: 13087–13102.
20. Tilmes S, Müller R, Salawitch R (2008) The sensitivity of polar ozone depletion to proposed geoengineering schemes. *Science* 320(5880):1201–1204.
21. Grodsky SA, et al. (2012) Haline hurricane wake in the Amazon/Orinoco plume: AQUARIUS/SACD and SMOS observations. *Geophys Res Lett* 39:L20603.
22. Bellenger H, Guilyardi E, Leloup J, Lengaigne M, Vialard J (2014) ENSO representation in climate models: From CMIP3 to CMIP5. *Clim Dyn* 42:1999–2018.
23. Wang CZ, Dong SF, Evan AT, Foltz GR, Lee SK (2012) Multidecadal covariability of North Atlantic sea surface temperature, African dust, Sahel rainfall, and Atlantic hurricanes. *J Clim* 25:5404–5415.
24. Booth BB, Dunstone NJ, Halloran PR, Andrews T, Bellouin N (2012) Aerosols implicated as a prime driver of twentieth-century North Atlantic climate variability. *Nature* 484:228–232.
25. Landsea CW, Franklin JL, Beven JL (2013) The revised Atlantic hurricane database (HURDAT2). United States National Oceanic and Atmospheric Administration's National Weather Service. Available at www.nhc.noaa.gov/data/hurdat/hurdat2-format-atlantic.pdf. Accessed May 20, 2015.
26. Haywood JM, Jones A, Bellouin N, Stephenson D (2013) Asymmetric forcing from stratospheric aerosols impacts Sahelian rainfall. *Nat Clim Chang* 3:660–665.
27. Aquila V, Garfinkel CI, Newman PA, Oman LD, Waugh DW (2014) Modifications of the quasi-biennial oscillation by a geoengineering perturbation of the stratospheric aerosol layer. *Geophys Res Lett* 41:1738–1744.
28. Trepte CR, Veiga RE, McCormick MP (1993) The poleward dispersal of Mount Pinatubo volcanic aerosol. *J Geophys Res* 98:18563–18573.
29. McCormick MP, Thomason LW, Trepte CR (1993) Atmospheric effects of the Mt. Pinatubo eruption. *Nature* 373:399–404.
30. Young RE, Houben H, Toon OB (1994) Radiatively forced dispersion of the Mt. Pinatubo volcanic cloud and induced temperature perturbations in the stratosphere during the first few months following the eruption. *Geophys Res Lett* 21:369–372.
31. Hofmann DJ, Rosen JM (1985) Antarctic observations of stratospheric aerosol and high altitude condensation nuclei following the El Chichon eruption. *Geophys Res Lett* 12:13–16.
32. Bluth GJS, Doiron SD, Schnetzler CC, Krueger AJ, Walter LS (1992) Global tracking of the SO_2 clouds from the June 1991 Mount Pinatubo eruptions. *Geophys Res Lett* 19: 151–154.
33. Heckendorn P, et al. (2009) The impact of geoengineering aerosols on stratospheric temperature and ozone. *Environ Res Lett* 4:045108.
34. Niemeier U, Timmreck C (2015) What is the limit of stratospheric sulfur climate engineering? *Atmos Chem Phys Discuss* 15:10939–10969.
35. Kravitz B, et al. (2014) A multi-model assessment of regional climate disparities caused by solar geoengineering. *Environ Res Lett* 9(7):74013–74019.
36. Kennedy AB, Dietrich JC, Westerink JJ (2013) The surge standard for "events of Katrina magnitude". *Proc Natl Acad Sci USA* 110(29):E2665–E2666.
37. Grinsted A, Moore JC, Jevrejeva S (2013) Reply to Kennedy et al.: Katrina storm records in tide gauges. *Proc Natl Acad Sci USA* 110(29):E2667.
38. Hansen J, Ruedy R, Sato M, Lo K (2010) Global surface temperature change. *Rev Geophys* 48:RG4004.
39. Kravitz B, et al. (2011) The Geoengineering Model Intercomparison Project (GeoMIP). *Atmospheric Science Letters* 12:162–167.
40. Jones A, et al. (2013) The "termination effect" in experiment G2 of the Geoengineering Model Intercomparison Project (GeoMIP). *J Geophys Res* 118(17): 9743–9752.
41. Taylor KE, Stouffer RJ, Meehl GA (2012) An overview of CMIP5 and the experiment design. *Bulletin of the American Meteorological Society* 93:485–498.
42. Ji D, et al. (2014) Description and basic evaluation of Beijing Normal University Earth System Model (BNU-ESM) version 1. *Geoscience Model Development* 7:2039–2064.
43. Collins WJ, et al. (2011) Development and evaluation of an earth-system model—HadGEM2. *Geoscience Model Development* 4:1051–1075.
44. Dufresne J-L, et al. (2013) Climate change projections using the IPSL-CM5 earth system model: From CMIP3 to CMIP5. *Clim Dyn* 40:2123–2165.
45. Arora VK, et al. (2011) Carbon emission limits required to satisfy future representative concentration pathways of greenhouse gases. *Geophys Res Lett* 38:L05805.
46. Phipps SJ, et al. (2011) The CSIRO Mk3L climate system model version 1.0—Part 1: Description and evaluation. *Geoscience Model Development* 4:483–509.
47. Schmidt GA, et al. (2006) Present day atmospheric simulations using GISS Model E: Comparison to in-situ, satellite and reanalysis data. *J Clim* 19:153–192.
48. Watanabe S, et al. (2011) MIROC-ESM 2010: Model description and basic results of CMIP5-20c3m experiments. *Geoscience Model Development* 4:845–872.
49. Brown LD, Cai TT, DasGupta A (2001) Interval estimation for a binomial proportion. *Stat Sci* 16:101–133.

Supporting Information

Moore et al. 10.1073/pnas.1510530112

SI Results

We show results in Figs. S1 and S2 of temperature anomalies under *G3* and *G4* relative to the baseline *rcp45* climate based on the individual models listed in Fig. 2. Figs. S3 and S4 show individual GEV model simulations for *G3* and *G4* forced by temperature output from the models separately. Results for eight other tide gauge locations analogous to Fig. 4 are shown in Fig. S5.

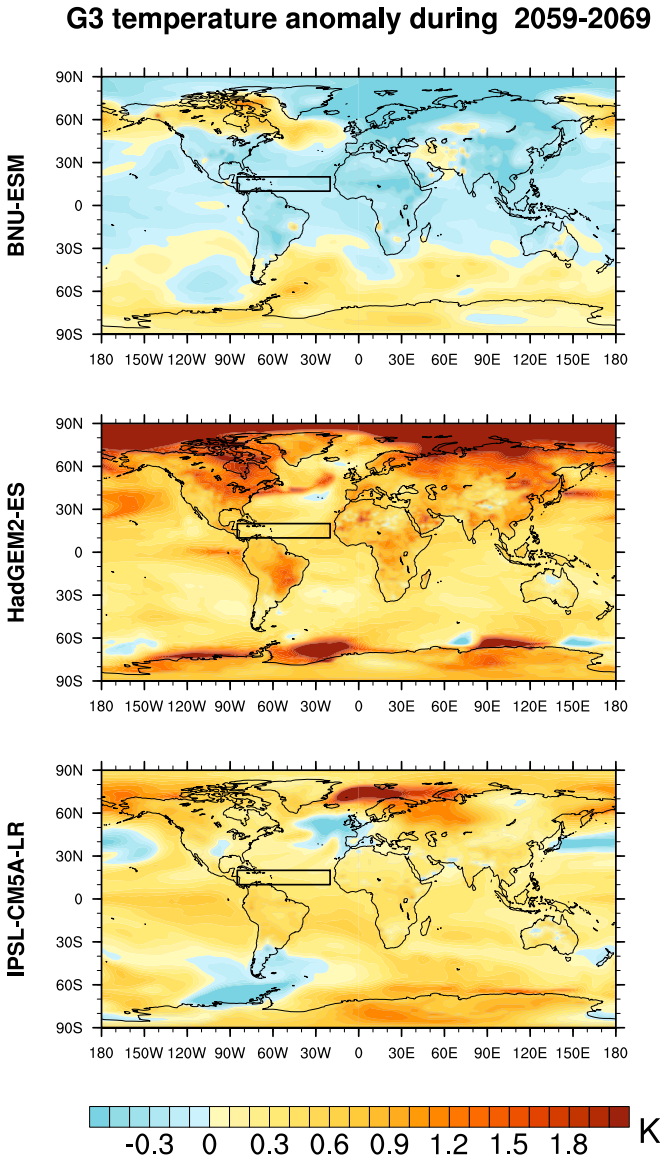

Fig. S1. Individual model simulations for surface air temperature anomalies under *G3* during 2050–2069 relative to the baseline *rcp45* climate state between 2010 and 2029; the MDR is marked by a black rectangle.

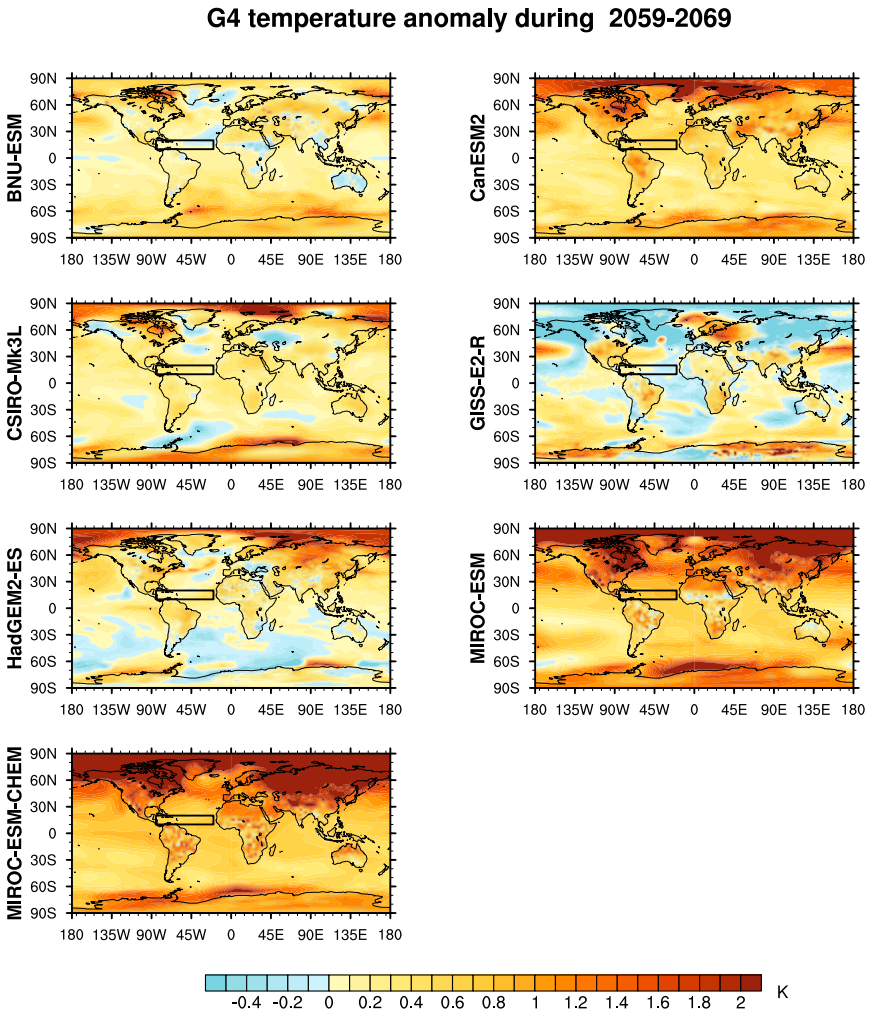

Fig. S2. Individual model simulations for surface air temperature anomalies under *G4,* during 2050–2069 relative to the baseline *rcp45* climate state between 2010 and 2029; the MDR is marked by a black rectangle.

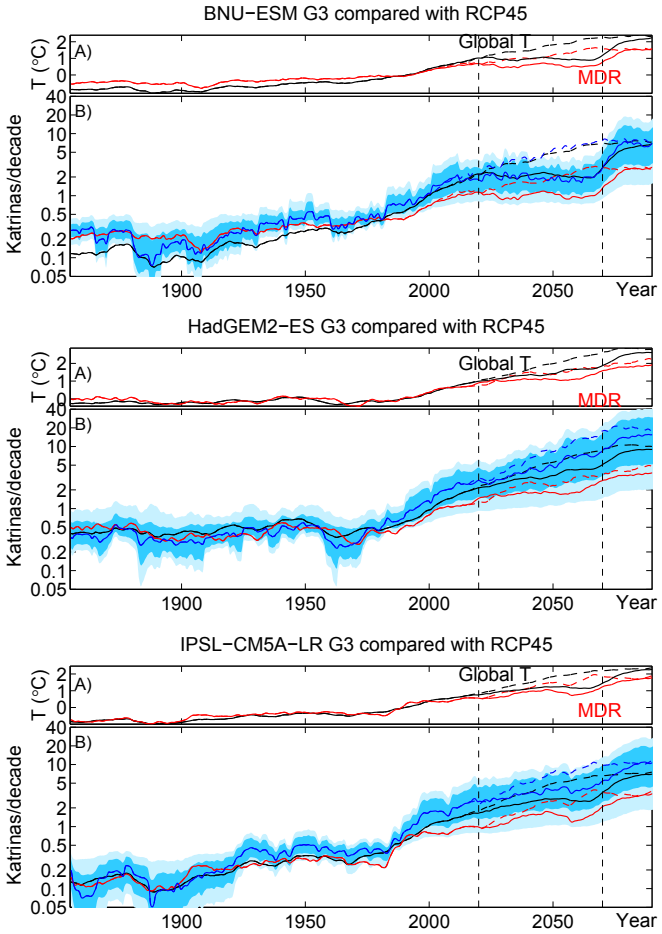

Fig. S3. Individual model earth system model-derived numbers of Katrina-magnitude surge events per decade (*B*) under the projected changes in temperatures modeled with the *G3* (*Bottom*) geoengineering simulations and the RCP4.5 forcing scenarios shown by the temperatures in *A*. The vertical dashed lines indicate the period 2020–2070 during which the geoengineering is applied. Solid lines indicate results under geoengineering, and dashed lines indicate results under RCP4.5; blue lines show the projection using the full spatial-gridded temperatures and confidence interval (5–16–84–95%); and red and black show the projections using only MDR and global average surface temperature, respectively.

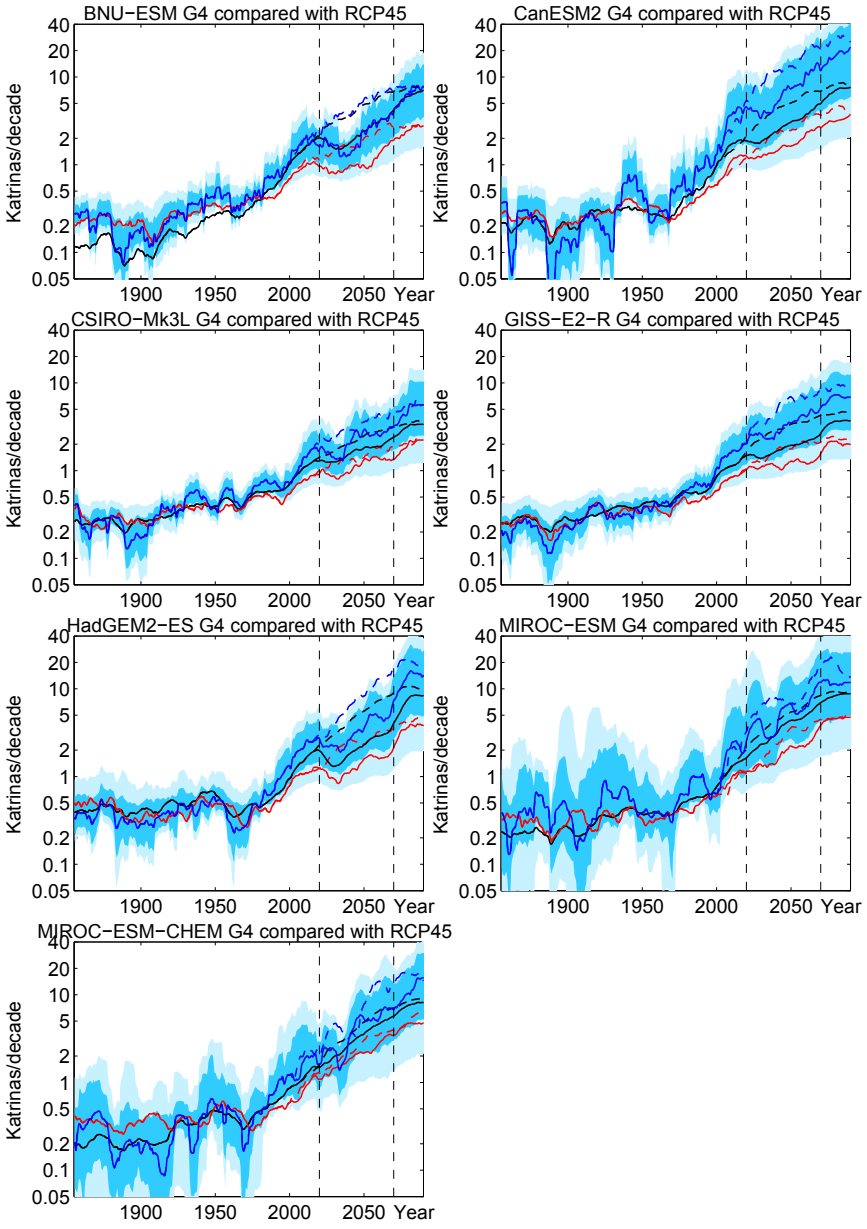

Fig. S4. Same as in Fig. S3*B*, but for *G4* models.

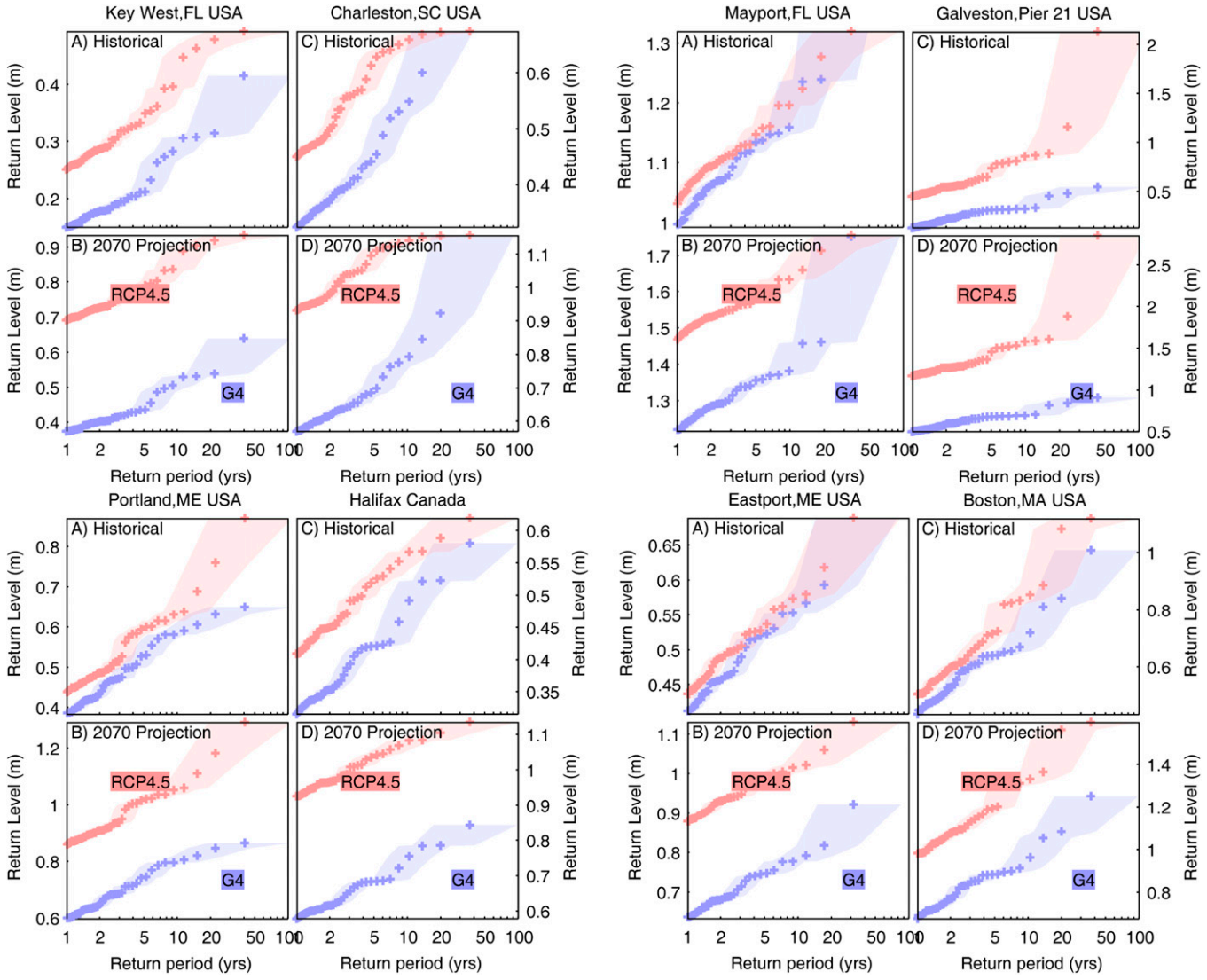

Fig. S5. Same as for Fig. 4, but for eight other cities with long-duration tide gauge data. (*Top*) For each city, the plot shows storm surge return periods from daily tide gauge data divided into globally relatively warm (red) and cool (blue) years, along with their 16–84% confidence ranges (shaded bands). (*Bottom*) For each city, the plot shows return period ranges at 2070 under RCP4.5 (red) and *G4* (blue) relative to mean sea level over 1990–2010. Return levels at 2070 were estimated taking into account local land subsidence, plus the 50th percentile rises forecast at each tide gauge site for 2070 under RCP4.5 (18) or *G4* (4).